The childhood of turbulent spot in shear flows

Marie Couliou, R. Monchaux

The childhood of turbulent spot in shear flows

M. Couliou[1, 2, *] and R. Monchaux[1]

[1] *IMSIA, ENSTA-ParisTech/CNRS/CEA/EDF, Université Paris Saclay, 828 Boulevard des Maréchaux, 91762 Palaiseau Cedex, France*
[2] *ONERA/DAAA, 8 rue des Vertugadins, 92190 Meudon, France*

We numerically investigate the temporal aspects of turbulent spot spreading in a plane Couette flow for transitional Reynolds numbers between 300 and 450. We focus our study on the spreading along the streamwise direction and on the shape of turbulent spots. Studying the topology of turbulent spots and the associated large-scale flows, we suggest a decomposition of the streamwise growth rate. On one hand, the quadrupolar large-scale flow heads for the spot along the streamwise direction and act against the growth. The associated growth rate is negative. On the other hand, we also define a positive growth rate associated to inside large-scale flow which enables the convection of the streaks. The sum of these two growth rates is compared to the spot streamwise growth rate and shows good agreement. The resulting shape of the spot is then discussed. A scenario gathering all these elements provides a better understanding of the growth dynamics and of the shape of a turbulent spot in a plane Couette flow. This scenario should be relevant to other shear flows.

PACS numbers:

I. INTRODUCTION

Transition to turbulence in wall-bounded shear flows has been subject of a wide range of studies over the last century. Turbulent spots, isolated regions of strong fluctuation within laminar flow are an essential feature of the transition. Depending on their dynamics, the final state of the flow can be a relaminarization, a permanent coexistence of both laminar and turbulent flows via stripe patterns or a homogeneously turbulent state. The existence of spots has been early reported in boundary layers by Emmons [14] who observed that localised perturbations move into organised spot. Long before, Reynolds [24] reported the apparition of intermittent flashes of irregular motion in his famous pipe flow experiment. Studying these flashes lately called slugs, Lindgren [19] measured the speed of their leading and trailing edges. Wygnanski *et al.* [28] observed sustained turbulent structure called puffs which can lead to slugs. Still in the configuration of a cylindrical pipe, a threshold Reynolds number can be defined by comparing the rates for puff decay and puff splitting (Avila et al [1]). The splitting process leads to the proliferation of turbulence while the decay drives the flow to the laminar state. The role of nonlinear advection in the growth of turbulent spots was also noted from a recent model of pipe and channel flows proposed by Barkley [2] and has been shown to play a crucial role in the growth of turbulent spots by Couliou & Monchaux [6] even if it is still difficult to take them into account in phenomenological models (Manneville [21]).

The present investigation focuses on the case of plane Couette flow (PCF), the flow which is sheared between two moving walls. The Reynolds number, being the natural control parameter, is defined as $Re = Uh/\nu$, where U and h are typical velocity and length scales, and ν is the fluid kinematic viscosity. A practical property of the PCF is that in a configuration of two counter-sliding plates, the flow has a zero advection speed enabling easier tracking of developing structures. This flow presents also many shared properties with other 2D flows as Taylor-Couette flow (flow between two rotating cylinders) and plane Poiseuille flow. The bidimensional extension of these flows leads to a more complex dynamics regarding the growth of turbulence patches called spots.

In the case of the PCF, Lundbladh & Johansson [20] made a few observations in their numerical simulations regarding the shape of the turbulent spot. The length L and the width l of the spot increase during the growth and as a function of the Reynolds number. The aspect ratio L/l increases during a first transitional period between 0 and 30 h/U (with h the half gap between the two walls and U the velocity of a wall) and then decreases. The ratio of the growth rate dL/dl decreases at short times and tends to 1 at long times. Regarding the spot shape, at short times, the spot has an elliptical shape and at longer times, the spot gets closer to a circle. The average growth rate of the spot in the spanwise direction is comparable to that found in the streamwise direction. Duguet *et al.* [13] have performed numerical simulations in a domain of great extension ($L_x = 800\ h$, $L_y = 2\ h$, $L_z = 365\ h$ with L_x, L_y, L_z, the dimensions of the domain in the steamwise, wall-normal and spanwise directions respectively). It corresponds to

*Electronic address: marie.couliou@onera.fr

approximately twelve times the domain extension used by Lundbladh & Johansson [20]. Duguet *et al*. [13] observed at short times a similar behaviour but at longer times they observe the emergence of an oblique stripe network before the extremities of the spot have reached the spanwise boundaries of the computational domain. Experimentally, Tillmark & Alfredsson [26, 27], Daviaud *et al*. [10] and Dauchot & Daviaud [8] observed the growth of triggered turbulent spots but with a focus on the subcritical nature of the transition when Dauchot & Daviaud [9] performed time-averaged growth rate measurements.

An early key element pointed out in the work of Lundbladh & Johansson [20] is the large-scale flow that develops around the turbulent growing spot with a quadrupolar structure. It has been observed numerically and experimentally in PCF [5, 12, 17] and is also present along the regular laminar/turbulent patterns [12]. This quadrupole has also been observed in model flows [4, 17, 25] and in other shears flows as in plane Poiseuille [18]. Couliou & Monchaux [6, 7] show the crucial role these large-scale flows have on the spot growth process along the spanwise direction. By using both experiments and direct numerical simulations, they have shown that two mechanisms are involved when turbulent spots grow along the spanwise direction : a formerly proposed local growth occurring at the spot spanwise tips but also in comparable proportion a global growth induced by large-scale advection.

In the spanwise direction, the large-scale flow enables the advection of the spot front. Since its shape is a quadrupole, its effect corresponds to expulsing flow at the spanwise edges of the spot and bring in flow at the streamwise edges, i.e large-scale flows should be acting against the growth of the turbulent spot in the streamwise direction. This assessment leads us to wonder which mechanism enables the propagation of the spot front in the streamwise direction.

In the present article, we focus on the spanwise growth and especially on the evolution of the spanwise spot front. Understanding how such an interface evolves in time and in space is the key for predicting wether turbulence would spread or not. To do so, we have run direct numerical simulations of growing spot at Re between 300 and 450. The generation and post-processing of these numerical data is described in section II. The main results consisting of the analysis of growth rates, front velocities and large-scale flow measurements are gathered in section III. Discussion of these results is givenin III followed by a summary of our findings and perspectives to this work.

II. METHODS

The x, y and z directions are respectively the streamwise, wall-normal and spanwise directions and U_x, U_y and U_z are the associated velocities. Velocities are made dimensionless using U, the normalised velocity of a wall, length by using h and times using h/U. The plane $y = 0$ corresponds to the mid-plane.

A. Direct numerical simulations

Direct Numerical Simulations of the Navier Stokes equations are computed in plane Couette geometry with the Channelflow code ([15, 16]) written by John F. Gibson. Pseudo-spectral methods are used for the spatial discretisation with a Fourier decomposition in the (x, z) directions and Chebyshev polynomials in y direction. The boundary conditions are periodic in the (x, z) directions and no slip conditions are imposed at the walls at $y = \pm 1$. The size of the domain is ($L_x = 180$, $L_y = 2$, $L_z = 80$) with a numerical resolution of (768, 33, 384) dealiased modes in the (x, y, z) directions. A time-step of 0.01 was used resulting in a CFL number less than 0.6. Four pairs of counter-rotating vortices as the one used in [20] is introduced as an initial disturbance to trigger turbulent spots. Five realisations of the DNS have been performed for each Re value and ensemble-averaged results are presented. Note that a slight change in the perturbation amplitude (typically 0.1%) is introduced to achieve variability between realisations.

B. Topology

The fields of U_x/U are represented in figure 1 in a plane close to $y = 1$, a slightly off-center plane close to $y = 0$ and in a plane close to $y = -1$. The laminar linear velocity profile have been subtracted. One can note the asymmetry of the spot in the direction normal to the plane. For planes close to $y = 1$ where $U_x \simeq 1$ (figure 1 .a), the spot is solely constituted of streaks with positive amplitude which are off-centered to the right of the spot ($x > 0$) while for planes close to $y = -1$ where $U_x \simeq -1$ (figure 1 .c), only streaks with negative amplitude are visible and all of these streaks are biased towards the left of the spot ($x < 0$). We also observe in planes close to $y = 0$ a symmetrical distribution of positive and negative streaks with respect to the $x = 0$ axis : negative streaks are rather observed in the left half ($x < 0$) while positive streaks prevail in the right half ($x > 0$).

A cut in the plane $z = 0$ as the one drawn in figure 1 allows to clarify this observation. Since the cut is realized in a $z = cste$ plane, a single pair of streaks is observed. On the right side of the spot ($x > 0$), the negative streaks are

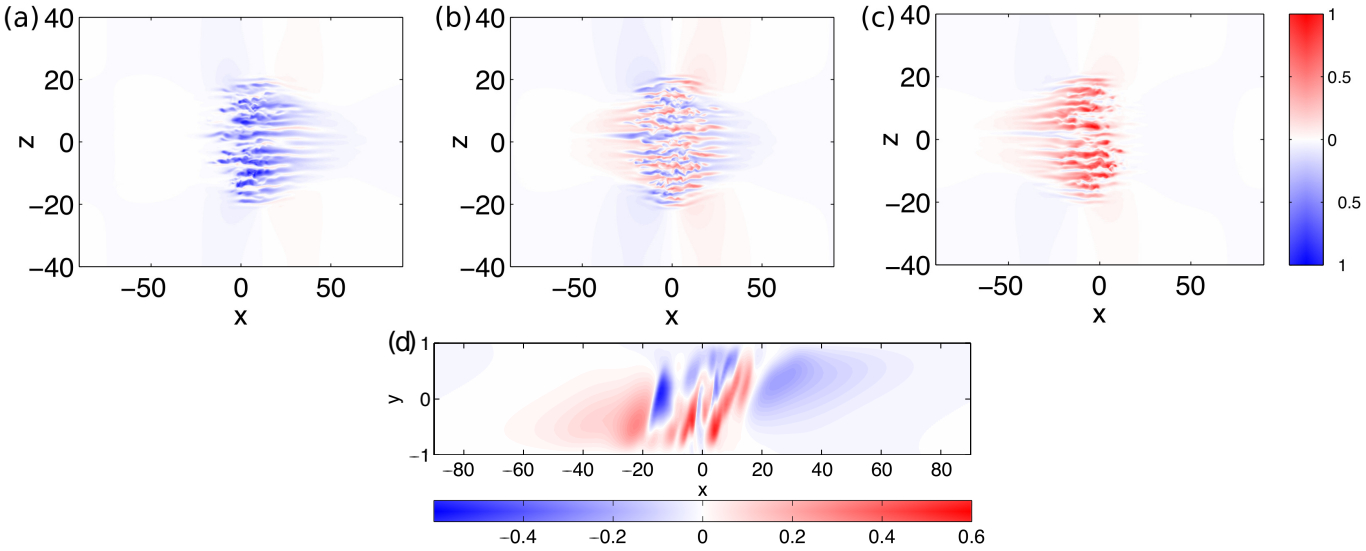

FIGURE 1: Top, from left to right : U_x velocity field at $Re = 360$ in the plane at $y = 0.77$, a slightly off-center plane at $y = 0.098$ and a plane at $y = -0.63$ at $t = 150$. Bottom : U_x velocity field at $Re = 360$ for $z = 0$ and $t = 150$

located in off-centered planes close to $y = 1$. Similarly, the positive streaks in off-centered planes close to $y = -1$ are located in the left of the spot ($x < 0$).

C. Detection method

Keeping in mind the 3D topology of a turbulent spot discussed above, the study is focused on a mid-plane in which both negative and positive streaks are captured. In order to mark the turbulent spot contour, U_x velocity fields are plotted. Two thresholds, T_h corresponding to an upper limit and T_b corresponding to a lower limit are defined. Pixels whose value is above T_h or below T_b correspond to positive streaks or negative streaks respectively. They are considered as turbulent and are set to 1. Pixels whose U_x level is between T_b and T_h correspond to laminar areas and are set to zero. A dilation erosion process is used to remove potential turbulent pixels considered laminar (false positive). The domain gathering pixels detected as turbulent is then closed to form a unique turbulent spot. Geometrical properties of the turbulent spot as its area, perimeter and aspect ratio can thus be easily deduced.

III. RESULTS

A. The shape of a turbulent spot

Figure 2 displays different snapshots taken along the growth of a turbulent spot. In a first phase, the spot is elliptic with the axis along the streamwise direction being longer than the axis along the spanwise direction. As the growth progresses, both principal axes tend to have the same length and the spot takes the shape of a more or less regular diamond whose sides form an angle with respect to the streamwise direction [13]. This angle is prefiguring the organized pattern orientation. The second phase is illustrated in the last snapshot of figure 2. Specific studies of this second phase are scarce. In very large domains, Duguet *et al.* [13] nevertheless present the typical evolution of a diamond-shaped spot turning progressively into a turbulent labyrinthine pattern made of several adjacent stripes with various orientations that are similar to the often described steady patterns. For a moderate size of the simulation domain as in our domain (when the spanwise direction is 40 times the distance between the walls), the spot size quickly becomes sizable with the domain spanwise extension and this second phase is nothing but a reorganization of the turbulent area into an inclined pattern. In the following, we focus on the first phase.

To quantify the growth, the turbulent fraction F_t corresponding to the ratio of the turbulent area to the total area of the domain is plotted in figure 3a. In the present paper, the turbulent area is exactly the area of the turbulent spot. Its evolution is divided into two phases. The time interval 0-60 corresponds to a common phase for every Re where the turbulent fraction increases from 0 to 0.004. Beyond t=60, the turbulent fraction still grows with time and the

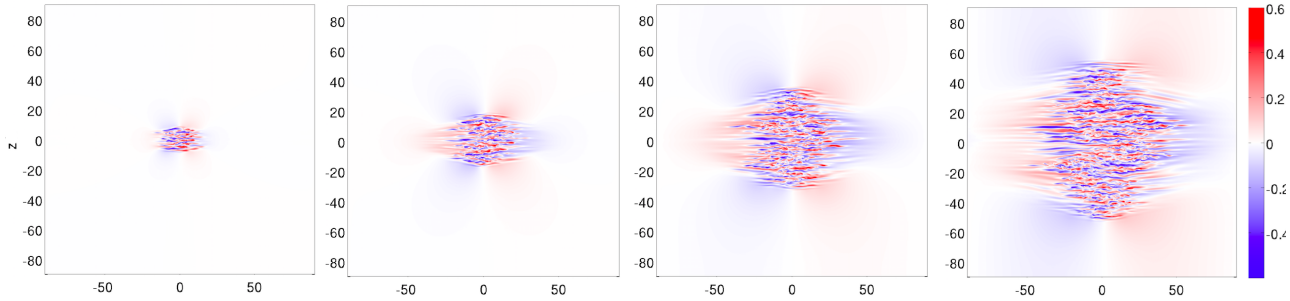

FIGURE 2: Temporal evolution of the turbulent spot at $Re = 380$. Successive snapshots of U_x respectively correspond to $t = 35$, $t = 108$, $t = 219$ and $t = 383$ after the initial perturbation.

growth rates are higher for higher Re.

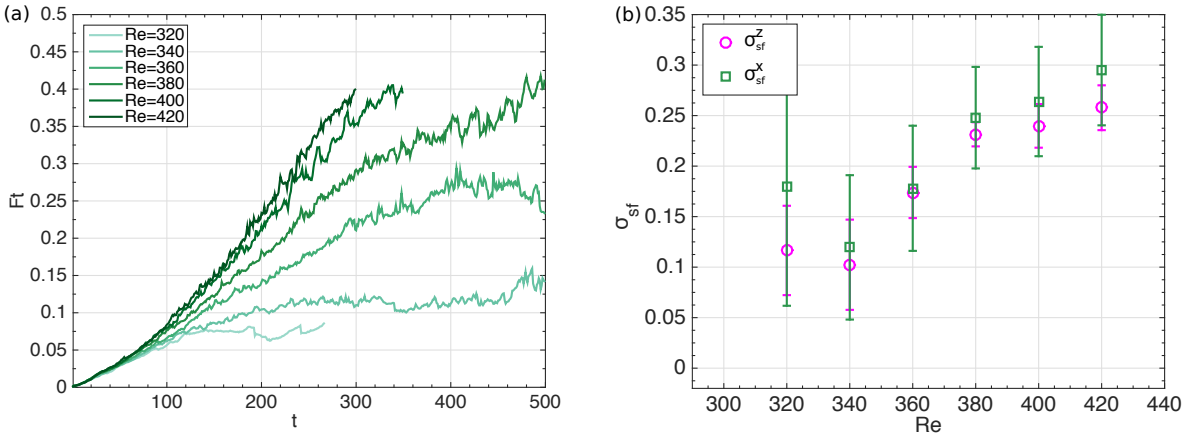

FIGURE 3: Temporal evolution of the turbulent fraction Ft for several Re and time-averaged spanwise front velocity $\overline{\sigma^z_{sf}}$ and time-averaged streamwise front velocity $\overline{\sigma^x_{sf}}$ as a function of Re.

We now focus on spot fronts and their velocities. The front of the spot is detected by a simple threshold on the velocity norm on the line $z = 0$ for the spanwise front and on the line $x = 0$ for the streamwise front. The determined front positions hardly depend on the chosen threshold. The average front position between several realizations at a given Re is obtained by cubic spline interpolations with smoothing parameter λ. This cubic spline is then differentiated to obtain the front velocity as a function of time. Several values of λ in a range between [0.5, 1] lead to slightly different velocity signals. These different signals are then time and ensemble-averaged to obtain the front-averaged velocity at a given Re. The corresponding standard deviation is used as an error bar.

The time-averaged streamwise front velocity $\overline{\sigma^x_{sf}}$ defined as the total of the front velocity from both left and right front of the spot and the time-averaged spanwise front velocity $\overline{\sigma^z_{sf}}$ defined as the total of the top and bottom front velocity are plotted in figure 3b. Regarding $\overline{\sigma^x_{sf}}$, the contribution of the left and right front velocities are equal and regarding $\overline{\sigma^x_{sf}}$, the contribution of the top and bottom front velocities are also found equal (not shown). By comparing $\overline{\sigma^z_{sf}}$ and $\overline{\sigma^x_{sf}}$ in figure 3, we observe almost equal time-averaged velocity along both directions, the difference being in the range of their errorbars. This result is quite surprising because the front dynamics is not the same along the two directions and we can also expect that the involved mechanisms along both directions are different. Over z the spot growth is indeed linked to the streak nucleation while over x the spot expansion is rather linked to an elongation of the streaks. This point will be discussed more in details in section IV. Few previous measurements enable to compare these values with other studies. In a half size domain compared to the one used in this present work, Lundblach & Johansson [20] measured the width of the spot for three Reynolds numbers ($Re = 375$, $Re = 750$ and $Re = 1500$) during 150 time units. For $Re = 375$, they found $\overline{\sigma^x_{sf}} \sim 0.17$ which is the same order of magnitude as in our study where $\overline{\sigma^x_{sf}}$ varies from 0.1 to 0.25 for Reynolds number between 340 and 420.

B. Front dynamics

In the spanwise direction, the expansion of the turbulent spot is understood as a succession of nucleations of new velocity streaks as detailed in [6, 7, 11]. In the streamwise direction, a streak occupies the entire spot length as can be seen in figure 1. The velocity distribution in the turbulent spot is plotted in figure 2 : we can see a distinct presence of negative streaks in the left half ($x < 0$) and of positive streaks in the right half ($x > 0$), in the central panel, large-scale flows directed within the spot both at its left and right sides can be clearly identified even without any spatial filtering. In term of velocity, we indeed observe outside of the spot that for $z \simeq 0$, U_x is negative for positive x and positive for negative x .

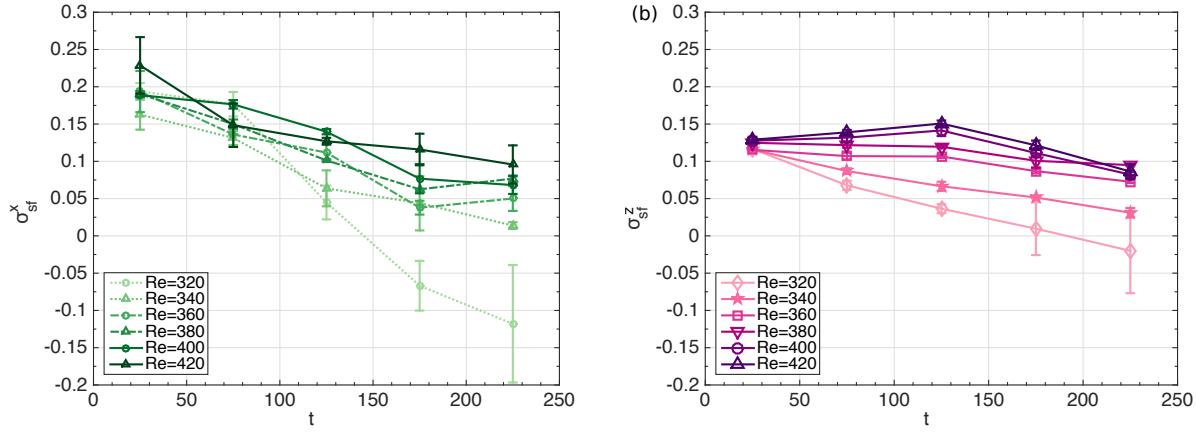

FIGURE 4: Streamwise front velocity σ^x_{sf} (a) and spanwise front velocity σ^z_{sf} (b) as a function of time for several Re

The evolution of the streamwise front velocity σ^x_{sf} is plotted as a function of time in figure 4a. For all Reynolds numbers, σ^x_{sf} decreases over time and all the more so as the Reynolds number is low. It is found that for short times (between t=0 and t=75), σ^x_{sf} is roughly independent of the Reynolds number. From t =125, the decrease of σ^x_{sf} is more pronounced for lower Re. For $Re = 320$, it gets negative which is a sign of a retreat of the spot rather than an expansion. Regarding σ^z_{sf} , it presents a maximum visible in figure 4b that is reached at about $t = 125$ whenever $Re > 360$. Below this value, it monotonously decreases with time, the lower the Reynolds number, the stronger the decreasing rate. The spreading rate ends up negative for $Re = 320$ because the spot vanishes. As a reminder, despite very different spatio-temporal dynamics visible in figure 4 between σ^z_{sf} (peak velocity at mid-growth) and σ^x_{sf} (monotonous decay in time)), we observe almost equal average speeds in figure 3b.

In a previous study [6], we have suggested a growth mechanism in the spanwise direction in which the spanwise front velocity is split into two contributions :

$$\sigma^z_{sf} = \sigma^z_{loc} + \sigma^z_{adv}, \tag{1}$$

with σ^z_{loc} a growth rate associated to a local streak nucleation mechanism and σ^z_{adv} a growth rate associated with a streak nucleation mechanism governed by the advection of the turbulent spot by the large-scale flows. Along the spanwise direction z, the quadrupolar large-scale flows pulling out flow of the turbulent spot have an advection role. Thus, in terms of order of magnitude σ^z_{adv} can be compared to a measure of the large scale flow intensity as :

$$\sigma^z_{adv} \sim max(U^z_{LSF})_{(x=0,z>0)}. \tag{2}$$

In a similar fashion, the following part is dedicated to large-scale flows and their potential effects on streamwise growth.

C. Large scale flows

Large-scale flows develop around growing turbulent spots in shear flows. As reported in [5, 12, 17], we identify them by studying the two-dimensional spatial power spectrum of either velocity component in the (x, z) plane where a scale separation between two peaks is visible. One peak of energy is around the wavelength $\lambda \simeq 4 - 5$ and is associated to

turbulent streaks. The second peak is associated to large scale flows and situated around $\lambda = 40$. A cut-off at $\lambda_c = 24$ enables to extract the large-scale and small-scale structures with 4^{th} order Butterworth low-pass and high-pass filters. Figure 5 shows snapshots of U_x associated with large scales (left) and small scales (right).

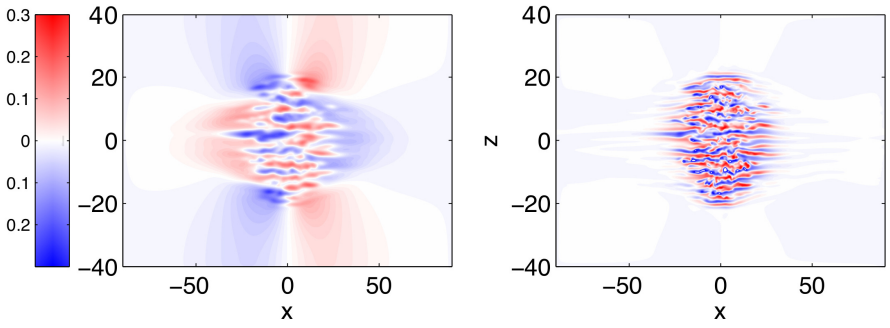

FIGURE 5: U_x at $Re = 360$ in the plane $y = 0$ at $t = 150$ for large-scale (left) and small-scale (right).

The expected quadrupole is visible with the low-pass filter for both U_x or U_z velocity component (U_z is not shown). Large-scale structures are also visible inside the turbulent spot itself on the U_x field. A left-right symmetry of this inside large-scale flow is noticeable : for the left part of the spot ($x < 0$), a strong negative U_x velocity component is prevailing while for the right part ($x > 0$), it is a strong positive U_x velocity component which is predominant. Regarding the small scales (figure 5 right), the streaks associated with edge vortices are visible at the border of the spot and the turbulent steaks are homogeneously observed in the entire turbulent spot.

Given the symmetries, we can restrict our study to only half the domain without any generality loss. We choose to focus on $x > 0$ where one observes intense outer large-scale flows with a negative streamwise velocity. In the same subdomain, within the turbulent spot, inner large-scale flows have a positive streamwise velocity. A local direct estimation of the intensity of outer large scale flows is realised by extracting the minimum value of the large-scale filtered streamwise velocity component $\min(U^x_{LSF})|_{(z=0,x>0)}$ together with $X_{\max}$, the position of this minimum large-scale velocity for $z \in [-20, 20]$. A local direct estimation of the intensity of inner large scale flows is the maximum large-scale velocity $\max(U^x_{LSF})|_{(z=0,x>0)}$ sought for the area $x > X_{min}$ in the same interval $z \in [-20, 20]$. Velocities are averaged over all realisations done at the same Reynolds number and are smoothed by averaging in time over five time steps. Velocities are plotted in figure 6. For the sake of clarity in the writing of min and max, the subscript $z = 0$ will be dropped.

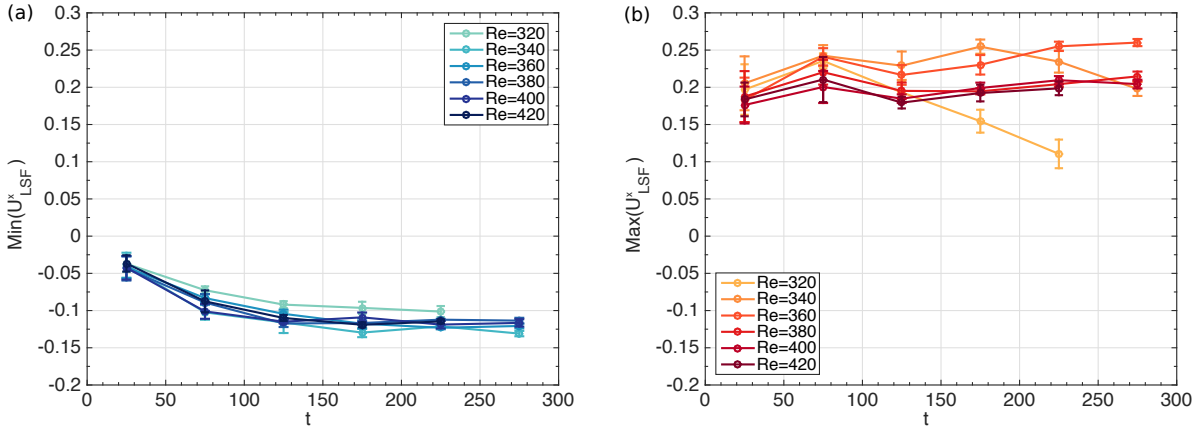

FIGURE 6: $\min(U^x_{LSF})|_{x>0}$ as a function of time for several Re and $\max(U^x_{LSF})|_{x>0}$ as a function of time for several Re

The evolution of $\min(U^x_{LSF})|_{x>0}$ on the line $z = 0$ is shown in figure 6a. For all Reynolds numbers, $\min(U^x_{LSF})|_{x>0}$ decreases with time from 0 to quickly reach a value of approximately -0.1 U. Then the overall trend for all Re is a slower decrease ; $\min(U^x_{LSF})|_{x>0}$ falls from -0.1 to -0.15 at $t = 250$. The evolution of $\max(U^x_{LSF})|_{x>0}$ is shown in figure 6b. For all Reynolds numbers, $\max(U^x_{LSF})|_{x>0}$ is roughly constant around 0.2.

IV. DISCUSSIONS

From the study of the topology of turbulent spot and the associated large-scale flow in section III, we suggest a decomposition of the streamwise growth rate as the sum of two rates σ^x_{inner} and σ^x_{outer} which are sketched in figure 7.

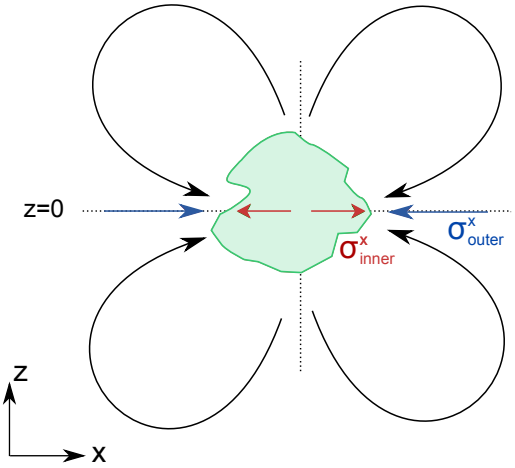

FIGURE 7: Sketch of the topology of a turbulent spot and of the associated large-scale flows.

On one hand, the quadrupolar large-scale flow steers inside the spot along the streamwise direction and slows down its growth. The associated growth rate is negative. We call σ^x_{outer} the rate representing the quadrupolar large-scale flow contribution which steers inside the spot at $z = 0$. In a first approximation, we can compare this rate to the minimum value of U^x_{LSF} around the line at $z = 0$ outside the spot which is a local estimation of the large-scale filtered velocity outside the spot :

$$\sigma^x_{outer} \sim \begin{cases} \min(U^x_{LSF})|_{x>0}, & \text{for } x > 0 \\ \max(U^x_{LSF})|_{x<0}, & \text{for } x < 0 \end{cases} \tag{3}$$

On the other hand, we define a positive growth rate σ^x_{inner} associated with the inside large-scale flow which enables the convection and the elongation of the streaks. σ^x_{inner} is compared in a first approximation to the maximal value of U^x_{LSF} around the line at $z = 0$ inside the spot, a local estimation of the large-scale filtered velocity inside the spot :

$$\sigma^x_{inner} \sim \begin{cases} \max(U^x_{LSF})|_{x>0}, & \text{for } x > 0 \\ \min(U^x_{LSF})|_{x<0}, & \text{for } x < 0 \end{cases} \tag{4}$$

The sum of these two growth rates, $\sigma^x_{inner} + \sigma^x_{outer}$ is compared to the spot streamwise growth rate σ^x_{sf}. Using the approximation formula from equations 3 and 4, we can directly compare $\max(U^x_{LSF})|_{x>0} + \min(U^x_{LSF})|_{x>0}$ to σ^x_{sf}. This is done in figure 8. Both quantities have a time evolution in two parts : an initial decrease of the rate until $t \sim 100 - 150$ followed by a slowdown and even a plateau at later times and higher Reynolds numbers. The range of positive values of σ^x_{sf} is slightly higher (0 to 0.22) than the one of $\sigma^x_{inner} + \sigma^x_{outer}$ (0 to 0.18). Evolution and the values of $\sigma^x_{inner} + \sigma^x_{outer}$ show a reasonable agreement with those of σ^x_{sf}. This means that the decomposition we suggest, solely based on large-scale contributions, captures a reasonable part of the mechanisms involved in the streamwise growth, and all the more so when considering that maximum and minimum are very raw estimations of the large scale flow intensity.

Figure 9 shows the ratio between $\min(U^x_{LSF})|_{x>0}$ and $\max(U^x_{LSF})|_{x>0}$ as an estimation of the competition between the two growth rates σ^x_{inner} and σ^x_{outer}. The ratio increases until $t \simeq 100 - 150$ and then plateaus at 0.6. This initial growth is linked to the fact that the large scale flows slowly develop outside the spot along its growth while the inner mechanism remains roughly constant all along the dynamics as seen in figure 6. The time evolution of the ratio (increasing then saturating) is similar for all Re. The higher is Re, the quicker the plateau is reached. The ratio is always lower than 1 which is consistent with the fact that the turbulent spot is growing along the x direction.

From this study on the expansion of the turbulent spot in the streamwise direction and from the recall we have done regarding the expansion along the spanwise direction, we expand our study on the shape of the turbulent spot. We define l_x the length of the turbulent spot on the line $z = 0$ corresponding to the distance between the right and

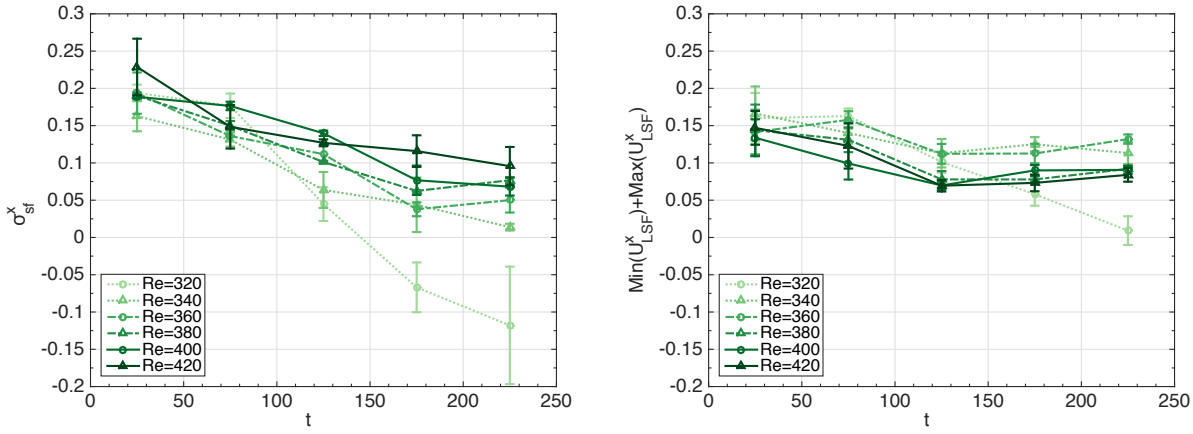

FIGURE 8: Evolution of the spot streamwise growth rate σ^x_{sf} and of $\max(U^x_{LSF})|_{(x>0)} + \min(U^x_{LSF})|_{(x>0)})$ as a function of time for several Re.

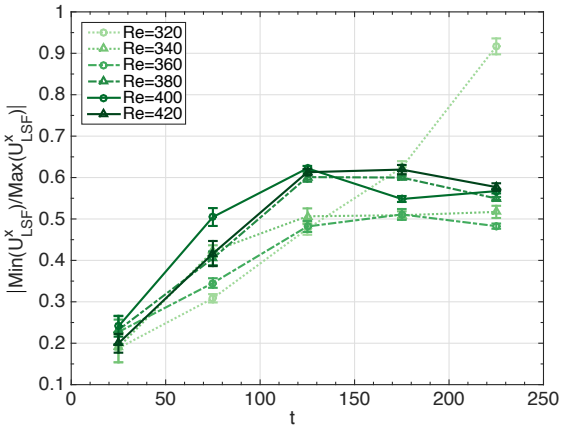

FIGURE 9: Time evolution of the ratio $|\min(U^x_{LSF})/\max(U^x_{LSF})|$ for several Re.

left front of the spot and l_z as the distance between the top edge and bottom edge on the line $x = 0$. Figure 10 represents the time evolution of the ratio l_x/l_z for different Reynolds numbers. The temporal evolution of l_x/l_z can be divided into three phases. The $t = 0 - 75$ interval is a common phase for every Re where the ratio triplicates from 0.5 to 1.5. The range $t = 75$-T_1 corresponds to a phase where l_x exceeds l_z but the ratio l_x/l_z decreases. T_1 is noted as the time when the ratio is equal to 1. T_1 is within $[150 - 270]$ and is getting shorter as the Reynolds number gets higher. Beyond T_1, the ratio stabilizes to values around 1. At longer times beyond $t = 350$, l_x/l_z may become less than 1 but this does not correspond to the first stage of the spot growth any more but rather to its reorganization.

The time evolution of the ratio l_x/l_z is obviously linked to the time evolution of the streamwise front velocity σ^x_{sf} and spanwise front velocity σ^z_{sf} shown in figure 4 in section III. The time averaged ratio l_x/l_z is around 1 which is consistent with the fact that the time-averaged spanwise front velocity $\overline{\sigma^z_{sf}}$ is equal to the time-averaged streamwise front velocity $\overline{\sigma^x_{sf}}$ for all Re (figure 3). To conclude, the shape of the spot can be explained by focusing on the evolution of the streamwise and spanwise spot fronts.

The impact of the domain size on the shape of the spot is now discussed. The ratio between the spanwise and the streamwise rate is affected by the domain size and the ratio of spanwise and streamwise directions. In a previous study [7], we have shown that the influence of the box size is negligible at the beginning of the growth, but becomes significant at later times when the effect of the periodic boundary conditions on the spot front is no longer negligible. In order to avoid any bias from this size effect, the spot growth dynamics is studied before the box size influences the spot development. More specifically, the recording of the front position should be stopped when it reaches 36h with our box size. We expect that the dynamics of shape and front are the same in larger domains for the range of time studied here. After this first period, previous works as Duguet *et al* [13] have enlightened that the spot have not

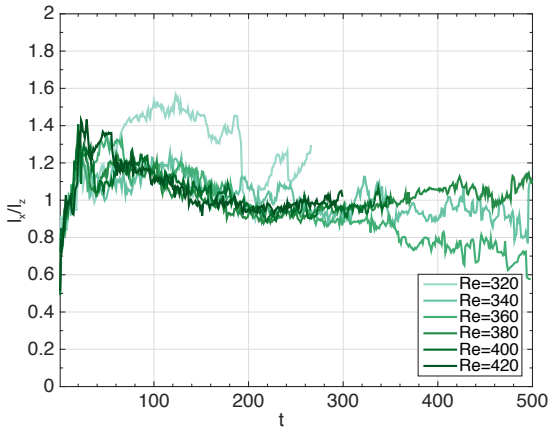

FIGURE 10: Temporal evolution of the ratio l_x/l_z for several Re.

anymore a diamond shape but turns into a network of intricated domains of inclined stripes with various orientations. In larger domains, the large-scale flow will remain but will not be affected by domain boundaries because it decays away from the spot. The ratio between each regimes (decrease/increase of σ^z_{sf}, etc) will not be anymore of the same order of magnitude. So the equal time-averaged spanwise and streamwise growth rates should not be true anymore.

The origin of the inner large-scale flow is unknown. The mechanism associated with the displacement of the streamwise front is also unclear. In a boundary layer flow, Matsubara & Alfredsson [23] show from flow visualizations that some elongated streaks appear and they suggest that a secondary instability is acting on the streaks. Brandt *et al* [3] suggest a convective instability of the streaks along the streamwise direction. The streak perturbation response is comprised of the sinuous mode of instability triggered by the spanwise wake-like profile. Streaks behave as flow amplifiers. The convective instability presents the ingredients to explain the elongation of streaks along the streamwise direction in a turbulent spot. The inner large-scale structure could be the signature of this instability. A deeper analysis as a more accurate estimation of the different contribution of the spanwise growth could help denying or confirming this hypothesis. Nevertheless, if the inner contribution comes from the streak instability described above, it should remain roughly constant in time, which is indeed the case as seen in figure 6.

Intense large-scale flows are observed in a laminar-turbulent coexistence with a stripe pattern in plane Couette flow by Duguet & Schlatter [12] and Manneville [22]. An interesting perspective would be to also establish the exact role of these large-scale structures in organizing and maintaining this pattern. This work provides a scenario that gives a better understanding of the growth dynamics and the shape of a turbulent spot in plane Couette flow and should possibly be extended to equilibrium states as the laminar turbulent stripes or be applied to other shear flows.

[1] K. Avila, D. Moxey, A. de Lozar, M. Avila, D. Barkley, and B. Hof. The Onset of Turbulence in Pipe Flow. Science, 333 :192–196, 2011.
[2] D. Barkley, B. Song, V. Mukund, G. Lemoult, M. Avila, and B Hof. The rise of fully turbulent flow. Nature, 526 :550–553, 2015.
[3] L. Brandt, C. Cossu, J.-M. Chomaz, P. Huerre, and D. S Henningson. On the convectively unstable nature of optimal streaks in boundary layers. Journal of Fluid Mechanics, 485 :221–242, 2003.
[4] M. Chantry, L. S. Tuckerman, and D. Barkley. Turbulent-laminar patterns in shear flows without walls. arXiv :1506.05002v2, 2016.
[5] M. Couliou and R. Monchaux. Large scale flows in transitional plane couette flow : a key ingredient of the spot growth mechanism. Phys. Fluids, 27 :034101, 2015.
[6] M. Couliou and R. Monchaux. Spreading of turbulence in plane couette flow. Phys. Rev. E, 93 :013108, 2016.
[7] Marie Couliou and Romain Monchaux. Growth dynamics of turbulent spots in plane couette flow. Journal of Fluid Mechanics, 819 :1–20, 2017.
[8] O. Dauchot and F. Daviaud. Finite-Amplitude Perturbation in Plane Couette Flow. Europhysics Letters, 28 :225–230, 1994.
[9] O. Dauchot and F. Daviaud. Finite amplitude perturbation and spots growth mechanism in plane Couette flow. Phys. Fluids, 7 :335–343, 1995.
[10] F. Daviaud, J. Hegseth, and P. Berge. Subcritical transition to turbulence in plane couette flow. Physical Review Letters,

69 :2511–2514, 1992.
[11] Y. Duguet, O. Le Maître, and P. Schlatter. Stochastic and deterministic motion of a laminar-turbulent front in a spanwisely extended Couette flow. Phys. Rev. E, 84 :066315, 2011.
[12] Y. Duguet and P. Schlatter. Oblique laminar-turbulent interfaces in plane shear flows. Phys. Rev. Lett., 110 :034502, 2013.
[13] Y. Duguet, P. Schlatter, and D. S. Henningson. Formation of turbulent patterns near the onset of transition in plane Couette flow. J. Fluid Mech, 650 :119–129, 2010.
[14] H. W. Emmons. The laminar-turbulent transition in a boundary layer. part1. J. Aero. Sc., 18 :490–498, 1951.
[15] J. F. Gibson. Channelflow : A spectral Navier-Stokes simulator in C++. Technical report, U. New Hampshire, 2014. `Channelflow.org`.
[16] J. F. Gibson, J. Halcrow, and P. Cvitanović. Visualizing the geometry of state space in plane Couette flow. J. Fluid Mech., 611 :107–130, 2008.
[17] M. Lagha and P. Manneville. Modeling of plane Couette flow. i. Large scale flow around turbulent spots. Phys. Fluids, 19 :094105, 2007.
[18] G. Lemoult, J.-L. Aider, and J.-E. Wesfreid. Turbulent spots in a channel : large-scale flow and self-sustainability. Journal of Fluid Mechanics, 731 :R1, 2013.
[19] E. R. Lindgren. Propagation velocity of turbulent slugs and streaks in transition pipe flow. The Physics of Fluids, 12(2) :418–425, 1969.
[20] A. Lundbladh and A. V. Johansson. Direct simulation of turbulent spots in plane couette flow. J. Fluid Mech., 229 :499–516, 1991.
[21] P. Manneville. Towards a model of large scale dynamics in transitional wall-bounded flows. arXiv :1504.00664, 2015.
[22] Paul Manneville. On the growth of laminar–turbulent patterns in plane couette flow. Fluid Dynamics Research, 44(3) :031412, 2012.
[23] M. Matsubara and P. H. Alfredsson. Disturbance growth in boundary layers subjected to free-stream turbulence. Journal of Fluid Mechanics, 430 :146–168, 2001.
[24] O. Reynolds. An Experimental Investigation of the Circumstances Which Determine Whether the Motion of Water Shall Be Direct or Sinuous, and of the Law of Resistance in Parallel Channels. Philosophical Transactions Series I, 174 :935–982, 1883.
[25] J. Schumacher and B. Eckhardt. Evolution of turbulent spots in a parallel shear flow. Phys. Rev. E, 63 :046307, 2001.
[26] N. Tillmark. On the Spreading Mechanisms of a Turbulent Spot in Plane Couette Flow. Euro Phys. Lett., 32 :481–485, 1995.
[27] N. Tillmark and P. H. Alfredsson. Experiments on transition in plane Couette flow. J. Fluid Mech., 235 :89–102, 1992.
[28] I. J. Wygnanski and F. H. Champagne. On transition in a pipe. part 1. the origin of puffs and slugs and the flow in a turbulent slug. Journal of Fluid Mechanics, 59(2) :281–335, 1973.